••

The break-up of heavy electrons at a quantum critical point

J. Custers[1], P. Gegenwart[1], H. Wilhelm[1], K. Neumaier[2], Y. Tokiwa[1], O. Trovarelli[1], C. Geibel[1], F. Steglich[1], C. Pépin[3] & P. Coleman[4]

[1]*Max-Planck-Institute for Chemical Physics of Solids, D-01187 Dresden, Germany*
[2]*Walther Meissner Institute for Low Temperature Research of the Bavarian Academy of Sciences, D-85748 Garching, Germany*
[3]*SPhT, L'Orme des Merisiers, CEA-Saclay, 91190 Gif-sur-Yvette, France*
[4]*CMT, Department of Physics and Astronomy, Rutgers University, Piscataway, New Jersey 08854-8019, USA*

....

The point at absolute zero where matter becomes unstable to new forms of order is called a quantum critical point (QCP). The quantum fluctuations between order and disorder[1–5] that develop at this point induce profound transformations in the finite temperature electronic properties of the material. Magnetic fields are ideal for tuning a material as close as possible to a QCP, where the most intense effects of criticality can be studied. A previous study[6] on the heavy-electron material YbRh$_2$Si$_2$ found that near a field-induced QCP electrons move ever more slowly and scatter off one another with ever increasing probability, as indicated by a divergence to infinity of the electron effective mass and scattering cross-section. But these studies could not shed light on whether these properties were an artefact of the applied field[7,8], or a more general feature of field-free QCPs. Here we report that, when germanium-doped YbRh$_2$Si$_2$ is tuned away from a chemically induced QCP by magnetic fields, there is a universal behaviour in the temperature dependence of the specific heat and resistivity: the characteristic kinetic energy of electrons is directly proportional to the strength of the applied field. We infer that all ballistic motion of electrons vanishes at a QCP, forming a new class of conductor in which individual electrons decay into collective current-carrying motions of the electron fluid.

Recent work[6] on the heavy electron material YbRh$_2$Si$_2$ (ref. 9) has demonstrated that a magnetic field can be used to probe the heavy electron QCP. This material exhibits a small antiferromagnetic (AFM) ordering temperature $T_N = 70$ mK (Fig. 1a) that is driven to zero by a critical magnetic field $B_c = 0.66$ T (if the field is applied parallel to the crystallographic c axis, perpendicular to the easy magnetic plane)[6]. For $B > B_c$, a field-induced Landau–Fermi liquid (LFL) state characterized by $\Delta\rho = AT^2$ (where $\Delta\rho(T) = \rho(T) - \rho_0$ is the temperature-dependent part of the electrical resistivity) is established below some cross-over temperature $T_0(B)$ which grows linearly with field. The A coefficient, being proportional to the quasiparticle–quasiparticle scattering cross-section, was found to diverge as $A(B) \propto 1/(B - B_c)$ for $B \to B_c$. Comparative studies of the resistivity and the electronic specific heat $C_{el}(T) = \gamma_0(B)T$ in the field ranges 0.5–4 T (**B** ⊥ **c** with $B_c = 0.06$ T) and 2–6 T (**B**∥**c**) revealed a field-independent ratio A/γ_0^2 slightly smaller than the empirical Kadowaki–Woods ratio[10] that holds for LFL systems. This seemed to suggest a divergence of the effective quasiparticle mass with $1/(B - B_c)^{1/2}$ as $B \to B_c$. Here we report our observation of the divergence of the quasiparticle mass at a QCP, established very close to $B = 0$.

By alloying YbRh$_2$Si$_2$ with germanium, using a nominal concentration $x = 0.05$, we have been able to fine-tune the Néel temperature of this material and the critical field far closer to zero, to a point where we can now reliably probe the zero-field transition using field-tuning. The phase diagram for a high-quality YbRh$_2$(Si$_{0.95}$Ge$_{0.05}$)$_2$ single crystal is shown in Fig. 1b. Non-Fermi-liquid (NFL) behaviour dominates over a funnel-shaped region of the T–B phase diagram down to the lowest accessible temperature of

20 mK. The critical field has been suppressed to as low as $B_c = 0.027$ T (**B** ⊥ **c**). As in the undoped material, there is a broad cross-over regime between the NFL and field-polarized LFL regimes with a mean cross-over temperature T_0 that is seen to rise linearly with the field B. Very weak AFM order develops in the $x = 0.05$ sample below $T_N = 20$ mK, as evidenced by the extremely weak anomaly in the electronic specific-heat coefficient (Fig. 2a).

Past experience[7,8] suggested that a finite field QCP has properties which are qualitatively different to a zero-field transition, shedding doubt on the reliability of these measurements as an indicator of the physics of a quantum phase transition at zero field. However, the zero-field properties of YbRh$_2$(Si$_{1-x}$Ge$_x$)$_2$ above $T \approx 70$ mK for the undoped ($x = 0$) and doped ($x = 0.05$) crystals are essentially identical (Fig. 2a), suggesting that by suppressing the critical field we are still probing the same QCP. In both compounds, the a.c.-susceptibility follows a temperature dependence $\chi^{-1} \propto T^\alpha$ from 0.3 K to 1.5 K, with $\alpha = 0.75$ (ref. 11), and the coefficient of the electronic specific heat, $C_{el}(T)/T$, exhibits[9] a logarithmic divergence between 0.3 K and 10 K. However, in the low-T paramagnetic regime, that is, $T_N < T \lesssim 0.3$ K, the a.c.-susceptibility follows a Curie–Weiss law (inset of Fig. 2a) with a Weiss temperature
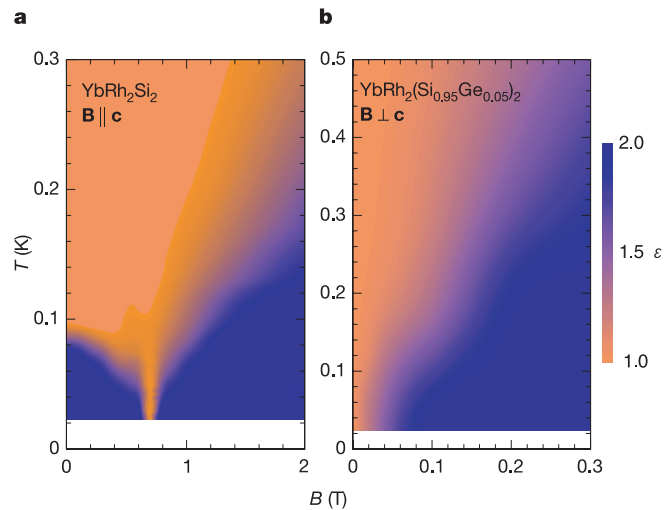

a   **b**

Figure 1 Evolution of ε, the exponent in $\Delta\rho(T) = [\rho(T) - \rho_0] \propto T^\varepsilon$, within the temperature–field phase diagram of YbRh$_2$(Si$_{1-x}$Ge$_x$)$_2$ single crystals. The non-Fermi-liquid (NFL) behaviour, $\varepsilon = 1$ (yellow), is found to occur at the lowest temperatures right at the QCP, $B = B_c$, and in a largely extended field range at higher temperatures. **a**, $x = 0$, $B_c = 0.66$ T (**B**∥**c**), residual resistivity $\rho_0 = 1$ μΩ cm; **b**, $x = 0.05$, $B_c = 0.027$ T (**B** ⊥ **c**), $\rho_0 = 5$ μΩ cm. For $B > B_c$, a broad cross-over regime from the NFL state to the field–induced heavy–LFL state (at lower temperature) occurs. The LFL state is characterized by $\Delta\rho(T) \propto T^\varepsilon$, $\varepsilon = 2$ (blue). As shown in **a** the antiferromagnetically ordered phase of pure YbRh$_2$Si$_2$ below $T_N = 70$ mK and B_c shows, owing to an extremely small ordered moment, the outward appearance of a heavy LFL state, too. Its phase boundary to the paramagnetic state is manifested by a rapid change in ε from 2 to 1. The low ordering temperature of pure YbRh$_2$Si$_2$ increases as external pressure is applied[9]. The extrapolation of $T_N(p) \to 0$ yields a critical pressure $p_c = -0.3(1)$ GPa, reflecting that a small expansion of the unit cell volume, V, would tune $T_N \to 0$. This can be achieved by the substitution of Si by the isoelectronic, but larger, Ge (ref. 16). Studies of the electrical resistivity under pressure revealed a $T_N \propto (p + p_c)^n$ variation, with $n = 1.33$ for both compounds. The $T_N(p)$ dependence of the $x = 0$ and $x = 0.05$ crystals can be matched if all $x = 0.05$ data points are shifted by the same amount $\Delta p = -0.17(2)$ GPa to lower pressure[16], yielding $T_N = 20(5)$ mK. Using the bulk modulus $B_0 = 189$ GPa of YbRh$_2$Si$_2$ (ref. 17), the small pressure shift of $\Delta p = -0.17(2)$ GPa is equivalent to a volume expansion of $\Delta V = 0.14(3)$Å^3. This transforms into an effective Ge content $x_{eff} = 0.019(6)$, if the value $\Delta V/V = 7.65(78)$% for the relative change of the unit-cell volume with Ge concentration in the solid-solution YbRh$_2$(Si$_{1-x}$Ge$_x$)$_2$ is used, with $V(x = 0) = 158.4(2)$Å^3 and $V(x = 1) = 166.07(54)$Å^3 (ref. 18) in agreement with microprobe analysis[11].

$\Theta \approx -0.3$ K, and a surprisingly large effective moment $\mu_{eff} \approx 1.4$ μ_B per Yb^{3+}, indicating the emergence of coupled, unquenched spins at the QCP. The electronic specific heat coefficient, $C_{el}(T)/T$, exhibits a pronounced upturn below 0.3 K.

We now discuss the field dependence of the electronic specific heat in $YbRh_2(Si_{0.95}Ge_{0.05})_2$ in more detail. In these measurements, magnetic fields were applied perpendicular to the crystallographic c axis, within the easy magnetic plane (Fig. 2b). At fields above 0.1 T, $C_{el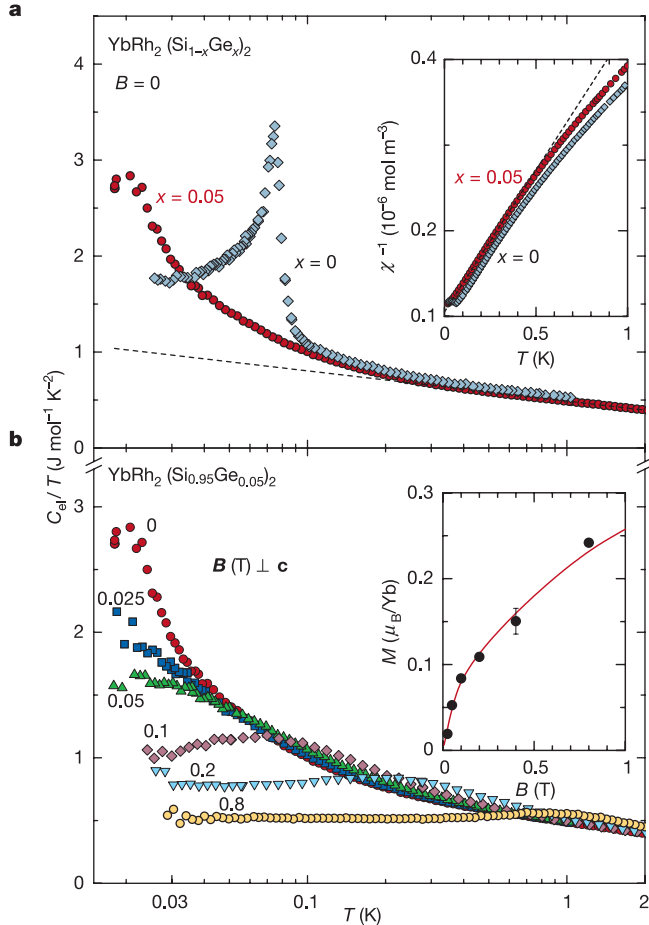}/T$ is almost temperature-independent, as expected in a LFL[12]. A weak maximum is observed in $C_{el}(T)/T$ at a characteristic temperature $T_0(B)$ which grows linearly with the field (inset of Fig. 3a), indicating that entropy is transferred from the low-temperature upturn to higher temperatures by the application of a field $B > B_c = 0.027$ T. As the field is lowered, the temperature window over which $C_{el}(T, B)/T = \gamma_0(B)$ is constant shrinks towards zero
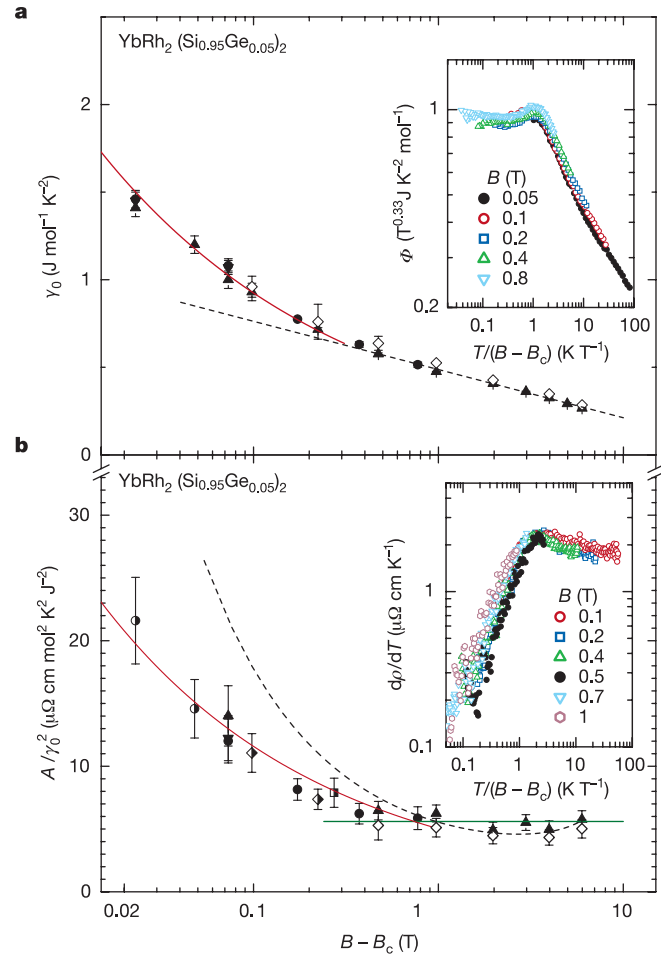

Figure 2 Low-temperature electronic specific heat of $YbRh_2(Si_{1-x}Ge_x)_2$ single crystals as C_{el}/T versus T in semi-logarithmic plots at zero field and at low values of the applied magnetic field B. Insets show low-T, $B = 0$, a.c.-susceptibility as χ^{-1} versus T (**a**) and magnetization as M versus B (**b**). C_{el} is obtained by subtracting the nuclear quadrupolar contribution, $C_Q = \alpha_Q/T^2$ (with $\alpha_Q = 5.68 \times 10^{-6}$ J K mol^{-1}, calculated from recent Mössbauer results[17]) (**a**) and, in addition, the nuclear Zeeman contribution $C_{hf} = \alpha(B)/T^2$ (**b**), from the raw data. Here, $\alpha(B)$ has been deduced by plotting CT^2 versus T^3 (**b**). The magnetization, M versus magnetic field B (black points in the inset to **b**), is calculated via $(B_{hf} - B)/a$, with a the hyperfine coupling constant for Yb in this compound and the hyperfine field $B_{hf} = ((\alpha(B) - \alpha_Q)/\alpha_{dip})^{1/2}$; α_{dip} represents the strength of the nuclear magnetic dipolar interaction and amounts to 7.58×10^{-8} J K mol^{-1} T^{-2} (ref. 19). With the assumption of $a = 120$ T/μ_B, the data points agree perfectly with the measured magnetization curve at 40 mK (red line in the inset to **b**). The $B = 0$ results shown in **a** reveal an upturn in $C_{el}(T)/T$ for paramagnetic $YbRh_2(Si_{1-x}Ge_x)_2$ ($x = 0$, $T_N = 70$ mK; $x = 0.05$, $T_N = 20$ mK) below $T = 0.3$ K. In the same temperature range the susceptibility $\chi(T)$ shows a Curie–Weiss law, $\chi^{-1} \propto (T - \Theta)$ (inset of **a**). For both samples very similar values are found for the Weiss temperature, $\Theta \approx -0.3$ K, as well as for the large effective moment, $\mu_{eff} \approx 1.4\mu_B$ per Yb^{3+}. For $YbRh_2(Si_{0.95}Ge_{0.05})_2$, entropy is shifted from low to higher temperatures when a magnetic field is applied (**b**). The cross-over temperature between the field-induced LFL state ($C_{el}(T)/T \approx$ const.) and the NFL state at higher temperature is depicted by the position of the broad hump in $C_{el}(T)/T$ which shifts upwards linearly with the field, $B \leq 0.8$ T (**B** $\perp$ **c**).

Figure 3 Field dependences of the Sommerfeld coefficient γ_0, of the electronic specific heat (**a**) and of the ratio of the A coefficient in the T^2 term of the electrical resistivity and γ_0^2 (**b**) for $YbRh_2(Si_{0.95}Si_{0.05})_2$. Note that γ_0 and A are proportional to the effective quasiparticle mass and the effective quasiparticle–quasiparticle scattering cross-section, respectively. The magnetic field was applied perpendicular to the c axis, and the applied field values are corrected, on the abscissae, by the value of the critical field, $B_c = 0.027$ T. The γ_0 values in **a** were obtained from two different samples: three independent measurements on sample 1 are displayed by closed symbols (circles, up and down triangles). The open diamonds show the results of measurements on sample 2. As $B \to B_c$, γ_0 diverges $\propto (B - B_c)^{-0.33}$ (red line), that is much more strongly than logarithmically (black dashed line). The symbols used in the semi-logarithmic plot $K = A/\gamma_0^2$ versus $(B - B_c)$ of **b** correspond to values for the electronic specific-heat coefficient shown in **a**. Half-filled circles (or squares) display data for which the A coefficient of the electrical resistivity was determined by extrapolating (or interpolating) $A(B - B_c)$ with respect to $(B - B_c)$. The half-filled diamond represents a point for which the γ_0 value was obtained by interpolation. The black dashed line indicates $K_{SDW} \propto [(B - B_c) \ln^2(B - B_c)]^{-1}$ for the 2D SDW scenario[13]. This is at strong variance from the (at $B - B_c < 0.3$ T) experimentally observed $K \propto (B - B_c)^{-1/3}$, arising from the stronger than logarithmic increase of γ_0 upon cooling (red line in **a**). For $(B - B_c) > 0.3$ T, K becomes field-independent within the error bars at a constant value of 5.4 $\mu\Omega$ cm mol^2 K^2 J^{-2} (green horizontal line in **b**). A similar high-field behaviour has been reported previously[6] on pure $YbRh_2Si_2$. We note that an almost identical value for K was found. Insets show the scaling behaviour of the low-T electronic specific heat where, according to equation (1), the ordinate is displaying $\Phi(B, T) = (B - B_c)^{0.33} C_{el}/T$, **a**, as well as of the temperature derivative of the electrical resistivity, $d\rho/dT$, **b**, as a function of $T/(B - B_c)$.

and the zero-temperature $\gamma_0(B)$ diverges (Fig. 3a). For example, in a field of 0.05 T a constant value $\gamma_0(B) \approx 1.54(7)$ J mol^{-1} K^{-2} only develops below 40 mK. These results indicate the formation of a field-induced LFL state at a characteristic scale $T \lesssim T_0(B)$. As the window of LFL behaviour is reduced towards zero, an ever-increasing component of the zero-field upturn in the specific heat coefficient is revealed in the temperature dependence. This confirms that the major part of the upturn in the specific heat coefficient observed in zero field is electronic in character, and must be associated with the intrinsic specific heat at the QCP.

This conclusion is also supported by the electrical resistivity data which reveal a field-dependent cross-over from a T-linear resistivity at elevated temperatures, to quadratic behaviour $\Delta\rho = A(B)T^2$ at sufficiently low temperatures. Most importantly, the data show that at low fields and temperatures, the same scale $T_0(b) \propto b$ (where $b = B - B_c$ is the deviation from the critical field) governs the cross-over from LFL to NFL behaviour in both the thermodynamics and the resistivity. This can be quantitatively demonstrated by noting that the finite field transport and specific-heat data collapse into a single set of scaling relations (see Fig. 3 insets):

$$\frac{C_V}{T} = \frac{1}{b^{1/3}} \Phi\left(\frac{T}{T_0(b)}\right), \quad \frac{d\rho}{dT} = F\left(\frac{T}{T_0(b)}\right) \quad (1)$$

where $\Phi(x) \approx (\max(x, 1))^{-1/3}$ and $F(x) \approx x/\max(x, 1)$. The NFL physics is described by the $x \to \infty$ ($T \gg T_0(b)$) behaviour of these equations, where $d\rho/dT$ is constant and $C_V/T \propto T^{-1/3}$. By contrast, the field-tuned LFL is described by the $x \to 0$ limit of these equations. Were there any residual pockets of LFL behaviour that were left unaffected by the QCP, we would expect a residual quadratic component in the resistivity, and the data would not collapse in the observed fashion. We are thus led to believe that the break-up of the LFL involves the entire Fermi surface.

From the second scaling relation in equation (1), we see that the A coefficient of the T^2 term to the resistivity diverges roughly with $1/b$, a result that is consistent with earlier measurements on pure YbRh$_2$Si$_2$ carried out further away from the QCP (ref. 6). Over the same range, the specific-heat coefficient $\gamma_0(b)$ grows as $b^{-1/3}$ (Fig. 3a). Notice that the field dependence at absolute zero temperature can be interchanged with the temperature dependence at $B = B_c$, but only in the upturn region. At high magnetic field deviations from the QCP, earlier measurement showed[6] that the Kadowaki–Woods ratio[10] $K = A/\gamma_0^2$ is approximately constant. Closer to the QCP, where the scaling behaviour is observed, $K = A/\gamma_0^2 \approx b^{-1/3}$ is found to contain a weak field dependence (Fig. 3b).

We now discuss the broader implications of our measurements. The observed divergence of both the A coefficient of the resistivity and the coefficient γ_0 of the T-linear specific heat certainly rule out a three-dimensional spin-density-wave (SDW) scenario, which predicts that both quantities will remain finite at sufficiently low temperature in the approach to a zero-field QCP ($B \to B_c \to 0$), but it can be used to gain insight into the underlying scattering mechanisms between the quasiparticles. In a two-dimensional (2D) SDW scenario, the scattering amplitude between two heavy electrons is severely momentum-dependent. When used to compute the transport relaxation rate, the SDW scenario leads to the result $A \propto 1/\kappa^2$, with κ the inverse correlation length[13]. The observed divergence in $A(b)$ would require $\kappa^2 \propto b$. However, the fluctuations of the soft 2D spin fluctuations produce only a weak logarithmic renormalization in the heavy electron density of states, measured by the specific-heat coefficient, $\gamma_0 \propto \ln(1/\kappa)$. Thus the 2D SDW scenario predicts a weak divergence in the T-linear specific heat, but a strongly field-dependent enhancement of the Kadowaki–Woods ratio in the approach to a QCP ($b \to 0$), given by:

$$\gamma_{SDW} \propto \ln(1/b) \quad \text{and} \quad K_{SDW} \propto \frac{1}{b \ln^2(b)}. \quad (2)$$

The strong violation of these predictions in our data, presented in

Fig. 3, rules out 2D spin fluctuations as the driving force behind the thermodynamics and the dominant source of scattering near the heavy electron QCP.

Taking a more general view, scaling behaviour of the transport scattering rate tells us that the only scale entering into the density of states and the scattering amplitude is the single scale $T_0 \propto b$ of the heavy electron fluid. A truly field-independent Kadowaki–Woods ratio would indicate that the quasiparticle scattering amplitude has the form:

$$A^\star = T_F^{\star 2} \mathscr{F}[\{k_{in}\} \to \{k_{out}\}]. \quad (3)$$

The weak field dependence of the Kadowaki–Woods ratio over a wide range of fields implies that the characteristic length scale of the most singular scattering amplitudes renormalizes more slowly in the approach to the QCP than expected in a SDW scenario.

Our data also provide some insight into the thermodynamics in the vicinity of the QCP. By integrating the scaling form (1) for the specific heat over temperature, the entropy $S(T) = \int_0^T dT'(C_V/T')$ in the vicinity of the QCP can be described by the form:

$$S(T, B) = b^{1-\eta} \mathscr{S}\left(\frac{T}{T_0(b)}\right) \quad (4)$$

where $\eta = 1/3$. The appearance of a field-dependent pre-factor in this equation forces the entropy to vanish at the QCP, as required by the third law of thermodynamics. The exponent in the pre-factor also determines the effective Fermi temperature $T_F^\star(b) \propto \gamma(b)^{-1} \propto T_0(b)^\eta$. Thus the requirement that the entropy vanishes at the QCP ($\eta < 1$) prevents a direct proportionality between the Fermi-temperature of the heavy LFL and the scale $T_0(b)$ governing the cross-over to NFL behaviour. It follows that the Fermi temperature and cut-off temperature $T_0(b)$ must obey a relationship of the form:

$$T_F^\star(b) = T_\Lambda \left(\frac{T_0(b)}{T_\Lambda}\right)^\eta \quad (5)$$

where T_Λ is an upper cut-off that we might identify with the single-ion Kondo temperature of the Yb^{3+} ions (≈ 25 K). Such a power-law renormalization of the characteristic energy scale would be expected in the presence of locally critical fluctuations that extend down from T_Λ to the infrared cut-off provided, in this case, by the magnetic field[14].

In this respect, our results support the conclusions recently drawn from earlier measurements on the quantum critical material CeCu$_{6-x}$Au$_x$ ($x = 0.1$) (ref. 15), and used in a recently proposed theory for quantum criticality[4], suggesting that the most critical scattering is neither three-, two- or even one-dimensional, but local—as if the most critical fluctuations in the underlying quantum phase transition are fundamentally 'zero dimensional' in character.

One of our most striking observations is that below $T \approx 0.3$ K where $\chi(T)$ follows a Curie–Weiss law, the electronic specific-heat coefficient $C_{el}(T)/T$ for both samples starts to deviate towards larger values, separating away from the $-\log T$ dependence that is valid[9] up to 10 K (Fig. 2a). This 'upturn' continues in the $x = 0.05$ sample down to approximately 20 mK, if the critical field of 0.027 T ($\mathbf{B} \perp \mathbf{c}$) is applied (Fig. 2b). We ascribe this intrinsically electronic feature to the critical fluctuations associated with the zero-field quantum phase transition that exists at a slightly larger Ge concentration. The unique temperature dependence of $C_{el}(T)/T$ for $T < 0.3$ K is disparate from the linear temperature dependence of the electrical resistivity which holds all the way from $\gtrsim 10$ K to $T \approx 10$ mK. Since the former (thermodynamic) quantity probes the dominating local $4f$ ('spin') part of the composite quasiparticles, while the latter (transport) quantity is sensitive to the itinerant conduction-electron ('charge') part, one may view the observed disparity as a direct manifestation of the break–up of the composite fermions in the approach to the QCP. □

1. Hertz, J. A. Quantum critical phenomena. *Phys. Rev. B* **14**, 1165–1184 (1976).
2. Millis, A. J. Effect of a nonzero temperature on quantum critical points in itinerant fermion systems. *Phys. Rev. B* **48**, 7183–7196 (1993).
3. Continentino, M. A. Quantum scaling in many-body systems. *Phys. Rep.* **239**, 179–213 (1994).
4. Si, Q., Rabello, S., Ingersent, K. & Smith, J. L. Locally critical quantum phase transitions in strongly correlated metals. *Nature* **413**, 804–808 (2001).
5. Coleman, P. & Pépin, C. What is the fate of the heavy electron at a quantum critical point? *Physica B* **312**, 383–389 (2002).
6. Gegenwart, P. *et al.* Magnetic-field induced quantum critical point in YbRh_2Si_2. *Phys. Rev. Lett.* **89**, 056402 (2002).
7. Heuser, K. *et al.* Inducement of non-Fermi-liquid behavior with a magnetic field. *Phys. Rev. B* **57**, R4198–R4201 (1998).
8. Stockert, O. *et al.* Pressure versus magnetic-field tuning of a magnetic quantum phase transition. *Physica B* **312-313**, 458–460 (2002).
9. Trovarelli, O. *et al.* YbRh_2Si_2: Pronounced non-Fermi-liquid effects above a low-lying magnetic phase transition. *Phys. Rev. Lett.* **85**, 626–629 (2000).
10. Kadowaki, K. & Woods, S. B. Universal relationship of the resistivity and specific heat in heavy-fermion compounds. *Solid State Commun.* **58**, 507–509 (1986).
11. Gegenwart, P. *et al.* Divergence of the heavy quasiparticle mass at the antiferromagnetic quantum critical point in YbRh_2Si_2. *Acta. Phys. Pol. B* **34**, 323–334 (2003).
12. Landau, L. D. The theory of a Fermi liquid. *Sov. Phys. JETP* **3**, 920–925 (1957).
13. Paul, I. & Kotliar, G. Thermoelectric behavior near the magnetic quantum critical point. *Phys. Rev. B* **64**, 184414 (2001).
14. Giamarchi, T., Varma, C. M., Ruckenstein, A. E. & Nozières, P. Singular low energy properties of an impurity model with finite range interactions. *Phys. Rev. Lett.* **70**, 3967–3970 (1993).
15. Schröder, A. *et al.* Onset of antiferromagnetism in heavy-fermion metals. *Nature* **407**, 351–355 (2000).
16. Mederle, S. *et al.* Unconventional metallic state in YbRh_2(Si_{1-x}Ge_x)_2—a high pressure study. *J. Phys. Condens. Matter* **14**, 10731–10736 (2002).
17. Plessel, J. *et al.* Unusual behavior of the low-moment mangetic ground-state of YbRh_2Si_2 under high pressure. *Phys. Rev. B* **67**, 180303 (2003).
18. Francois, M., Venturini, G., Marchêché, J. F., Malaman, B. & Roques, B. De Nouvelles séries de germaniures, isotopes de U_4Re_7Si_6, ThCr_2Si_2 et CaBe_2Ge_2, dans les systèmes ternaires R-T-Ge où R est un élément des terres rares et T ≡ Ru, Os, Rh, Ir: supraconductivité de LaIr_2Ge_2. *J. Less Common Metals* **113**, 231–237 (1985).
19. Carter, G. C., *et al.* in Metallic shifts in NMR. *Progress in Materials Science* Vol. 20, Part I, Ch. 9 (eds Chalmers, B., Christian, J. W. & Massalski, T. B.) 123–124 (Oxford, Pergamon, 1977).

Superconductivity phase diagram of Na_xCoO_2·1.3H_2O

R. E. Schaak[1], T. Klimczuk[1,2], M. L. Foo[1] & R. J. Cava[1,3]

[1]*Department of Chemistry, Princeton University, Princeton, New Jersey 08544, USA*
[2]*Faculty of Applied Physics and Mathematics, Gdansk University of Technology, Narutowicza 11/12, 80-952 Gdansk, Poland*
[3]*Princeton Materials Institute, Princeton University, Princeton, New Jersey 08540, USA*

The microscopic origin of superconductivity in the high-transition-temperature (high-T_c) copper oxides remains the subject of active inquiry; several of their electronic characteristics are well established as universal to all the known materials, forming the experimental foundation that all theories must address. The most fundamental of those characteristics, for both the copper oxides and other superconductors, is the dependence of the superconducting T_c on the degree of electronic band filling. The recent report of superconductivity[1] near 4 K in the layered sodium cobalt oxyhydrate, Na_{0.35}CoO_2·1.3H_2O, is of interest

owing to both its triangular cobalt–oxygen lattice and its generally analogous chemical and structural relationships to the copper oxide superconductors. Here we show that the superconducting T_c of this compound displays the same kind of behaviour on chemical doping that is observed in the high-T_c copper oxides. Specifically, the optimal superconducting T_c occurs in a narrow range of sodium concentrations (and therefore electron concentrations) and decreases for both underdoped and overdoped materials, as observed in the phase diagram of the copper oxide superconductors. The analogy is not perfect, however, suggesting that Na_xCoO_2·1.3H_2O, with its triangular lattice geometry and special magnetic characteristics, may provide insights into systems where coupled charge and spin dynamics play an essential role in leading to superconductivity.

Like the high-T_c superconductors, the Na_xCoO_2·1.3H_2O crystal structure[1] consists of electronically active planes (in this case, edge-sharing CoO_6 octahedra) separated by layers (in this case, Na_x·1.3H_2O) that act as spacers, to yield electronic two-dimensionality, and also act as charge reservoirs (see below). We have found that varying the Na content in Na_xCoO_2·1.3H_2O results in the same type of out-of-plane chemical doping control of in-plane electronic
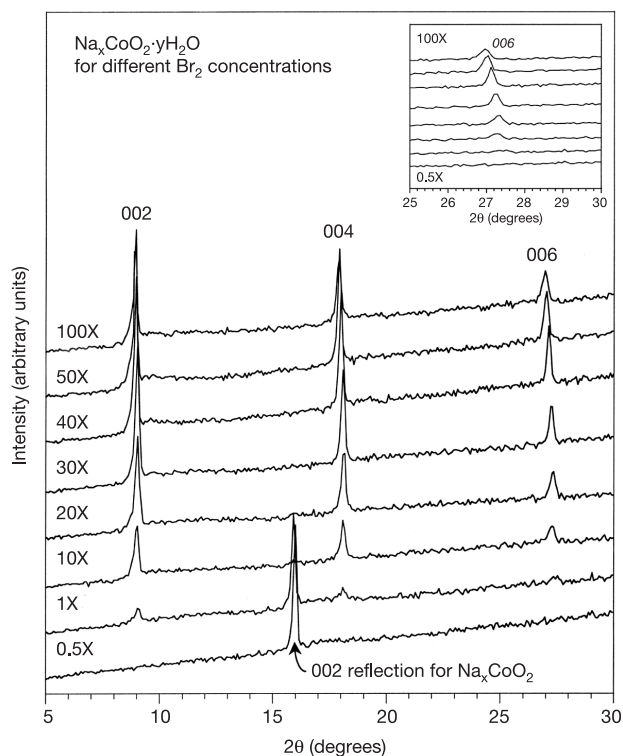

Figure 1 Powder X-ray diffraction patterns (Cu Kα radiation) for Na_xCoO_2·yH_2O samples prepared using different concentrations of the bromine de-intercalant. Inset, an enlargement of the 006 reflections for each sample, highlighting the shift in the layer spacing as a function of sodium content. The Na_xCoO_2·yH_2O samples were prepared by chemically de-intercalating sodium from Na_{0.7}CoO_2 using bromine as an oxidizing agent. Na_{0.7}CoO_2 (0.5 g) was stirred in 20 ml of a Br_2 solution in acetonitrile at room temperature for five days. Bromine concentrations representing substoichiometric (0.5×), stoichiometric (1×), and molar excess (10–100×) relative to sodium content were employed. ('1×' indicates that the amount of Br_2 used is exactly the amount that would theoretically be needed to remove all of the sodium from Na_{0.7}CoO_2.) The product was washed several times with acetonitrile and then water, and then dried briefly under ambient conditions. The sodium content of the phases was determined by the inductively coupled plasma atomic emission spectroscopy (ICP-AES) method. Very high Na diffusion coefficients facilitate homogenization of the Na contents of the samples at ambient temperature.